Physica A 703 (2026) 132168



Contents lists available at ScienceDirect

Physica A

journal homepage: www.elsevier.com/locate/physa



On the evolution of thermo-electromagnetic state of a superconductor with a Heat-Coupled extension of Time-Dependent Ginzburg–Landau model☆

Erhan Coşkun

Department of Mathematics, Karadeniz Technical University, TR-61080, Trabzon, Turkiye

ARTICLE INFO

Keywords:
Heat-coupled Ginzburg–Landau model
Method of planes
Superconductor
Thermo-electromagnetic state

ABSTRACT

The isothermal time-dependent Ginzburg–Landau model studied in our earlier works was coupled with an appropriately formulated heat equation that takes into account temperature dependence of specific heat, thermal conductivity and Ginzburg–Landau parameter with a source term representing Joule heating due to normal current. The parameters are chosen from niobium. The resulting Heat-Coupled Model(HTDGL) was numerically integrated with what we call 'method of planes' using high-order integration schemes of ODESUITE. Numerical experiments shed light on temporal evolution of thermo-electromagnetic state of superconductor. In particular, it was shown that both zero-field(ZF) and field-cooled(FC) procedures lead to stationary configuration of vortices having hexagonal pattern, as observed experimentally, with almost the same Abrikosov constant. Furthermore, it was observed that magnetic field penetration in FC procedure induces normal current around the boundary of sample, which in turn leads to rise of temperature near the edges in early stages of temporal evolution. Oscillatory applied field versus average temperature hysteresis loop shows that vortex motion leads to local increase of temperatures for both pure and impure superconductors with pinning sites and that interaction with pinning sites plays the greater role in thermal fluctuations due to induced local Joule heat. Fluctuations in the number of vortices were also observed under oscillatory field.

1. Introduction

The electromagnetic features of mesoscopic superconductors, whose sizes are of the same order as their penetration depth and coherence length, have been studied using both stationary and time-dependent Ginzburg–Landau models(GL and TDGL for short, respectively) [1–5]. TDGL, which is relatively simple compared to microscopic models, is known to be valid for conventional superconductors and gives reasonable picture of superconducting dynamics [6]. In addition to various theoretical studies concerning existence, uniqueness and regularity properties, the model has also been investigated numerically, in particular with finite elements [7–13] and the so-called nonstandard finite difference methods [14–19]. Though not closely related to the work here, various other forms of GL equations have been proposed and investigated in the literature, see for example, [20–24]. Optimization techniques [25] or parallel environments with multiprocessors have also been used to investigate models on relatively larger domains [26–29].

Reduced temperature-dependent isothermal extensions of the TDGL have also been proposed to investigate the thermo-electromagnetic features of superconductors [30], where it was shown that cooling speed strongly affects vortex dynamics. The

☆ This article is part of a Special issue entitled: 'Smart Airport Hub' published in Physica A.

E-mail address: erhan@ktu.edu.tr.

https://doi.org/10.1016/j.physa.2026.132168

Available online 17 October 2026
0378-4371/© 2026 Elsevier B.V. All rights are reserved, including those for text and data mining, AI training, and similar technologies.

so-called Extended TDGL is proposed in [23] to study oscillations in the magnitude and phase of order parameter, where TDGL is obtained in the limit case. A recent work on TDGL analyses Nb_3Sn type superconducting Radio-Frequency cavities and their performance in terms of Sn-deficient islands with an open-source finite element software called FEniCS [31]. Likewise TDGL is also used to study the finite frequency electrodynamics of superconductors subjected to intense spatially non-uniform of magnetic field created by a point magnetic dipole where the model is numerically solved using COMSOL Multiphysics [32]. However, isothermal models do not account for complete thermo-electromagnetic features because they assume a constant temperature irrespective of thermal effects associated with vortex motion and also disregard thermal effects that may influence electromagnetic features.

To help understand the thermo-electromagnetic state of a superconductor, various non-isothermal extensions of the TDGL model, referred to as non-isothermal or Heat-Coupled models(HTDGL), have also been proposed to supplement isothermal models with appropriately formulated heat equations. An HTDGL model was introduced in [33], where the only source term of heat equation was the temporal relaxation of the order function. The model was analysed further in [34] to prove its existence and uniqueness, and to provide some asymptotic results. HTDGL with a more complicated heat equation was proposed independently in [35,36], and was analysed further in [37] where existence and uniqueness results were given in addition to results showing the effect of time-varying currents and magnetic fields on the thermal properties of a thermally insulated sample with simulations in a zero-field cooling process with a gauge in terms of vector field and temperature. Another important work in this regard is [38]. The effect of heat dissipation on the current–voltage characteristics of a mesoscopic superconducting sample with leads has been studied in a recent study [39] where, among other good results, it was shown that heat dissipation leads to hysteresis in the current–voltage characteristics of superconducting wires, films or mesoscopic samples by using another variant of HTDGL with an ohmic heat source term with constant specific heat and thermal conductivity. Another model with a heat equation involving only the Joule heat source term with constant specific heat and thermal conductivity for a thin-film superconductor was considered in [40] to show that vortex–antivortex collision leads to the production of Joule heat. A model with ohmic and latent heat source terms was studied in [41], where channelling and branching of vortex penetration paths during flux avalanches were investigated with constant specific heat and thermal conductivity. Finally, we mention a recent study [42] that describes the role of the heat equation in simulating the resistive state of superconducting films.

This work supplements the relatively simple isothermal model studied in [30] with a heat equation having a single source term representing Joule heating, but unlike the previous works mentioned above, considers specific heat, thermal conductivity and Ginzburg–Landau parameter as a function of temperature based on physical experimental results of niobium superconductors, and simulates cooling of the sample under an applied field, the so-called field-cooling(FC), and cooling in the absence of applied field, the so-called zero-field-cooling(ZFC) through convective heat transfer process through the boundary. The resulting model was spatially discretized with a second-order nonstandard finite difference scheme and integrated efficiently and accurately using the method of planes strategy proposed in [43,44] with high-order integration schemes of ODESUITE [45]. Hexagonal pattern of vortices were observed for both cooling strategies with almost the same Abrikosov constant under constant applied field. Furthermore, it was observed that the GL energy functional, even for the HTDGL model, is a decreasing function until the equilibrium state in case of FC, but not in ZFC procedures. Normal currents that develop initially near the boundary of the sample under constant applied field increase the temperature locally and then drop because of the removal of heat through the lateral surfaces. Thermal effects under oscillatory field become more visible for samples with impurities where local increase of temperatures due to interaction of flux lines with impurities. To the best of the author's knowledge, the numerical simulations presented here are the first to simulate both FC and ZFC procedures of a superconductor based on the Heat-Coupled Ginzburg–Landau model which yields almost perfect hexagonal configurations in stationary state, implying global minimizer of related energy functional.

The remainder of this paper is organized as follows. In Section 2, for the sake of completeness, following [30] we introduce nonstandard scales and obtain non-dimensionalized temperature-dependent GL energy. In Section 3, we formulate an HTDGL model with Joule heat source term. Considering empirical findings based on niobium, temperature dependence of specific heat, thermal conductivity and GL parameter was taken into account. In Section 4, spatial discretization procedure and numerical integration algorithm implementing 'method of planes' approach of our previous works [43,44] was outlined and adapted for HTDGL. In Section 5, results of numerical simulations representing thermo-electromagnetic features of both FC and ZFC procedures under constant applied field were illustrated, in addition to features behind hysteresis curves under oscillatory field for samples with and without pinning sites.

2. GL energy in nondimensional units

The thermo-electromagnetic state of a superconductor in the form of a long(in z−direction) cylinder occupying a region, $\Omega \subset R^3$ and subject to an applied magnetic field $\mathbf{H}_o = (0, 0, H_o)^T$ can be described by a triple $(\Psi, \mathbf{A}, T)$ where Ψ is the complex-valued order function; $|\Psi|^2$ represents density of superconducting electrons; $\mathbf{A} = (A, B, 0)$ is the magnetic vector potential; $\mathbf{B} = \nabla \times \mathbf{A}$ is the magnetic field; T is the temperature, all of which can be assumed to vary along the x–y plane of sample's rectangular cross-section and depend on time t. We assume the sample is long enough in z−direction to justify considering variations only across the cross-section.

First, we consider the free energy functional(see [1]) with temperature T as a function of spatial coordinates, instead of being treated as a parameter(see [30]):

$$F(\Psi, \mathbf{A}, T) = \int_\Omega \left(\alpha(T)|\Psi|^2 + \frac{\beta(T)}{2}|\Psi|^4 + \frac{1}{2m^*}\left| \left(\frac{\hbar}{i}\nabla - \frac{e^*}{c}\mathbf{A} \right)\Psi \right|^2 + \frac{|\nabla \times \mathbf{A}|^2}{8\pi} - \frac{\nabla \times \mathbf{A}}{4\pi} \cdot \mathbf{H}_o \right) d\Omega, \tag{1}$$

where e^* and m^* are the effective values of the mass and charge of the superconducting electrons, respectively; c is the speed of light; i is the complex unity; $\hbar$ is the reduced Planck constant; $\alpha(T)$ changes sign at $T = T_c$(the critical temperature), with $\alpha(T) < 0$ for $T < T_c$, and $\beta(T) > 0$ for all $T > 0$.

The first two terms in (1) represent condensation energy density, while the second and last terms represent kinetic and field energy densities. In Gaussian unit system each term has the dimension of $m\ell^{-1}t^{-2}(m : mass, \ell : length, t : time)$, keeping in mind that energy has the dimension of $m\ell^2t^{-2}$. On the other hand, Ψ in d dimensional system has the dimension of $\ell^{-d/2}$. Using [.] to represent the dimension of the quantity inside the bracket, we have $[\Psi] = \ell^{-3/2}$ so that

$$\begin{aligned}
\left[|\Psi|^2\right] &= \ell^{-3}(\text{density:number per volume}),\\
[\alpha(T)] &= m\ell^2t^{-2} \text{ so } \left[\alpha(T)|\Psi|^2\right] = m\ell^{-1}t^{-2}\\
[\beta(T)] &= m\ell^5t^{-2}, \text{so } \left[\beta(T)|\Psi|^4\right] = m\ell^{-1}t^{-2}\\
\left[\mathbf{H}_o\right] &= [\nabla \times \mathbf{A}] = m^{1/2}\ell^{-1/2}t^{-1} \text{so } [\mathbf{A}] = m^{1/2}\ell^{1/2}t^{-1}.
\end{aligned} \tag{2}$$

In reduced units with T' representing T/T_c, we have(see [3])

$$\alpha(T') = (T' - 1)\alpha_0(T'), \tag{3}$$

where

$$\alpha_0(T') = \alpha_0(0)\frac{T'+1}{T'^2+1}, \quad \alpha_0(0) = \frac{e^{*2}}{m^*c^2}H_c(0)^2\lambda(0)^2. \tag{4}$$

Also,

$$\beta(T') = \frac{\beta(0)}{(1+T'^2)^2}, \ \beta(0) = \frac{4\pi e^{*4}}{m^{*2}c^4}H_c(0)^2\lambda(0)^4, \tag{5}$$

where $H_c(0)$ and $\lambda(0)$ are the thermodynamical critical field and London penetration depth at $T = 0$. Now, following [3,30], we let:

$$|\overline{\Psi_0(T')}|^2 = \frac{\alpha_0(T')}{\beta(T')}, \quad \overline{\lambda(T')} = \left(\frac{m^*}{4\pi|\overline{\Psi_0(T')}|^2}\right)^{1/2}\frac{c}{e^*}, \overline{\xi(T')} = \left(\frac{\hbar^2}{2m^*\alpha_0(T')}\right)^{1/2} \tag{6}$$

and $\overline{H_c(T')} = \left(4\pi\alpha_0(T')|\overline{\Psi_0(T')}|^2\right)^{1/2}$, where $|\Psi_0(T')|^2$, $\lambda(T')$, and $H_c(T')$(the thermodynamical critical field) are defined as above without the overbars on the right-hand sides. The reason we use $\alpha_0(T')$ in nondimensionalization instead of $\alpha(T')$, as done conventionally, is to disclose temperature dependence of the model(see [30] for details).

We check that dimensions of the quantities

$$\begin{aligned}
\left[|\overline{\Psi_0(T')}|^2\right] &= \left[\frac{\alpha_0(T')}{\beta(T')}\right] = \frac{m\ell^2t^{-2}}{m\ell^5t^{-2}} = \ell^{-3},\\
\left[\overline{\lambda(T')}\right] &= \left[\left(\frac{m^*}{4\pi|\overline{\Psi_0(T')}|^2}\right)^{1/2}\frac{c}{e^*}\right] = \left(\frac{m}{\ell^{-3}}\right)^{1/2}\frac{\ell t^{-1}}{m^{1/2}\ell^{3/2}t^{-1}} = \ell,\\
\left[\overline{H_c(T')}\right] &= \left[\left(4\pi\alpha_0(T')|\overline{\Psi_0(T')}|^2\right)^{1/2}\right] = (m\ell^2t^{-2}\ell^{-3})^{1/2} = m^{1/2}\ell^{-1/2}t^{-1},
\end{aligned} \tag{7}$$

likewise $\left[\overline{\xi(T')}\right] = \ell$, as $[\hbar] = m\ell^2t^{-1}$. We then use the following scales for non-dimensionalization which are slightly different from conventional ones due to overbars

$$\mathbf{x}' = \mathbf{x}/\bar{\lambda}, t' = t/t_0, t_0 = 4\pi\sigma_n\bar{\lambda}^2/c^2, \Psi' = \frac{\Psi}{\overline{\Psi}_0}, \mathbf{A}' = \frac{1}{\bar{\lambda}\bar{H}_c\sqrt{2}}\mathbf{A}, \ \mathbf{H}'_o = \frac{\mathbf{H}_o}{\sqrt{2}\bar{H}_c}, \tag{8}$$

and

$$F'(\Psi', \mathbf{A}', T') = \frac{F(\Psi', \mathbf{A}', T')}{\bar{\lambda}^2\alpha_0|\overline{\Psi}_0|^2}.$$

where σ_n is the normal conductivity coefficient with dimension of t^{-1} in Gaussian CGS system. We also note that

$$\bar{\kappa} = \frac{\bar{\lambda}}{\bar{\xi}} = \frac{\lambda}{\xi} = \kappa, \tag{9}$$

which follows from conventional definitions of

$$\lambda = \left(\frac{m^*}{4\pi|\Psi_0|^2}\right)^{1/2}\frac{c}{e^*}, \xi = \left(\frac{\hbar^2}{2m^*|\alpha|}\right)^{1/2} \text{ and the scale } |\Psi_0|^2 = \frac{\alpha}{\beta}. \tag{10}$$

It can be shown that, as explained in [30] in detail, non-dimensional energy functional over sample cross-section, by omitting primes, can be written as

$$F(\Psi,\mathbf{A},T)=\int_{\overline{\Omega}}\left[(T-1)|\Psi|^2+\frac{1}{2}|\Psi|^4+\left|\left(\frac{1}{i\kappa(T)}\nabla-\mathbf{A}\right)\Psi\right|^2+\left|\nabla\times\mathbf{A}-\mathbf{H}_o\right|^2\right]d\overline{\Omega}, \tag{11}$$

where $\overline{\Omega}=[0,L_x/\bar{\lambda}]\times[0,L_y/\bar{\lambda}]$ is the cross-section of nondimensional domain and from temperature dependence of [3]

$$\lambda(T)=\frac{\lambda(0)}{\sqrt{1-T^4}},\xi(T)=\frac{\xi(0)}{\sqrt{1-T}}(\text{see }) \tag{12}$$

we approximate

$$\kappa=\kappa(T)=\frac{\kappa(0)}{\sqrt{(1+T)(1+T^2)}}\approx\kappa(0)(1-T/2). \tag{13}$$

where it is seen that $\kappa(T)$ has limitations and is meaningful only for $T\in[0,1]$.

3. Heat coupled and time-dependent GL (HTDGL)

For isothermal model where T is treated as a temperature, the Ψ and $\mathbf{A}$ components of GL in zero-electric potential gauge [46] can be written as [30,47]

$$\eta\frac{\partial\Psi}{\partial t}=-\frac{\delta F}{\delta\Psi^*},\quad \sigma_n\frac{\partial\mathbf{A}}{\partial t}=-\frac{1}{2}\frac{\delta F}{\delta\mathbf{A}}. \tag{14}$$

where η is assumed to be nondimensional constant taken to be equal to one and normal conductivity coefficient σ_n is equal to one in the chosen system of units with time scale t_0 defined in (8), so we have

$$\frac{\partial\Psi}{\partial t}=\left((1-T)-|\Psi|^2\right)\Psi-\left(\frac{i}{\kappa(T)}\nabla+\mathbf{A}\right)^2\Psi, \tag{15}$$

$$\frac{\partial\mathbf{A}}{\partial t}=-\nabla\times(\nabla\times\mathbf{A})+\frac{1}{2\kappa(T)i}(\Psi^*\nabla\Psi-\Psi\nabla\Psi^*)+\mathbf{A}|\Psi|^2, \tag{16}$$

where (16) states in nondimensional form that total current density is equal to that of normal and supercurrent parts.

As stated above, this model does not take into account the interaction between thermal and electromagnetic effects, thus needs to be generalized to be more realistic. To this end we will treat T as a function of spatial and temporal variables. As for the governing equation for T, we state differential form of conservation of thermal energy, i.e., $\rho c_p(T)T$, as

$$\frac{\partial(\rho c_p(T)T)}{\partial t}+\nabla\cdot Q=S \tag{17}$$

where

$$Q=-k(T)\nabla T \tag{18}$$

is the heat flux with thermal conductivity $k(T)$; ρ is the density, $c_p(T)$ is the temperature dependent specific heat per unit volume and

$$S=\mathbf{J}_n\cdot\mathbf{E} \tag{19}$$

is ohmic heat per unit volume per unit time, where $\mathbf{E}$ is the electric field and

$$\mathbf{J}_n=\sigma_n\mathbf{E} \tag{20}$$

is the normal current. In zero potential gauge that eliminates scalar field we have

$$\mathbf{E}=-\frac{1}{c}\frac{\partial\mathbf{A}}{\partial t} \tag{21}$$

so that

$$\mathbf{J}_n\cdot\mathbf{E}=\frac{\sigma_n}{c^2}\left|\frac{\partial\mathbf{A}}{\partial t}\right|^2. \tag{22}$$

Thus, Eq. (17) becomes

$$\frac{\partial(\rho c_p(T)T)}{\partial t}=\nabla\cdot(k(T)\nabla T)+\frac{\sigma_n}{c^2}\left|\frac{\partial\mathbf{A}}{\partial t}\right|^2 \tag{23}$$

We nondimensionalize thermal conductivity by that of normal state, denoted by $k_n(T)$, and specific field by its value at normal state at $T=T_c$, denoted by $c_n(T_c)$:

$$k(T)=k_n(T)k'(T')\doteq k_n(T_c)k'(T'),c_p(T)=c_n(T_c)c_p'(T') \tag{24}$$

and note that $\nabla \to \frac{1}{\bar{\lambda}}\nabla$, so each term in Eq. (23) becomes

$$\frac{\partial(\rho c_p(T)T)}{\partial t} = \frac{\partial(\rho c_n(T_c)c_p'(T')T'T_c)}{\partial(t_0 t')} = \frac{\rho c_n(T_c)T_c}{t_0}\frac{\partial(c_p'(T')T')}{\partial t'}, \tag{25}$$

$$\nabla\cdot(k(T)\nabla T) = \frac{k_n(T_c)T_c}{\bar{\lambda}^2}\nabla\cdot(k'(T')\nabla T'), \tag{26}$$

$$\frac{\sigma_n}{c^2}\left|\frac{\partial \mathbf{A}}{\partial t}\right|^2 = \frac{\sigma_n}{c^2}\left|\frac{\bar{\lambda}\overline{H_c}\sqrt{2}\partial\mathbf{A}'}{\partial(t_0 t')}\right|^2 = \frac{2\sigma_n\bar{\lambda}^2\overline{H_c}^2}{c^2 t_0^2}\left|\frac{\partial\mathbf{A}'}{\partial t'}\right|^2. \tag{27}$$

Substituting (25), (26) and (27) in (23) we have

$$\frac{\rho c_n(T_c)T_c}{t_0}\frac{\partial(c_p'(T')T')}{\partial t'} = \frac{k_n(T_c)T_c}{\bar{\lambda}^2}\nabla\cdot(k'(T')\nabla T') + \frac{2\sigma_n\bar{\lambda}^2\overline{H_c}^2}{c^2 t_0^2}\left|\frac{\partial\mathbf{A}'}{\partial t'}\right|^2 \tag{28}$$

or

$$\frac{\partial(c_p'(T')T')}{\partial t'} = \frac{t_0 k_n(T_c)}{\rho c_n(T_c)\bar{\lambda}^2}\nabla\cdot(k'(T')\nabla T') + \frac{2\sigma_n\bar{\lambda}^2\bar{H}_c^{\,2}}{\rho c_n(T_c)T_c c^2 t_0}\left|\frac{\partial\mathbf{A}'}{\partial t'}\right|^2. \tag{29}$$

Dropping primes in (29), we have non-dimensionalized and nonlinear heat equation

$$\frac{\partial(c_p(T)T)}{\partial t} = c_d\nabla\cdot(k(T)\nabla T) + c_s\left|\frac{\partial\mathbf{A}}{\partial t}\right|^2 \tag{30}$$

with non-dimensional parameters

$$c_d = \frac{t_0 k_n(T_c)}{\rho c_n(T_c)\bar{\lambda}^2} = \frac{4\pi\sigma_n k_n(T_c)}{c^2\rho c_n(T_c)}, c_s = \frac{2\sigma_n\bar{\lambda}^2\overline{H_c}^2}{\rho c_n(T_c)T_c c^2 t_0} = \frac{1}{2\pi}\frac{\overline{H_c}^2}{\rho c_n(T_c)T_c}. \tag{31}$$

We can check the dimensions of the parameters in (31) to make sure that they are indeed dimensionless with $\theta = [T]$:

$$\begin{aligned}[(\sigma_n)(k_n(T_c))] &= (t^{-1})(m\ell t^{-3}\theta^{-1}) = m\ell t^{-4}\theta^{-1},\\ [(c^2)(\rho)(c_n(T_c))] &= (\ell^2 t^{-2})(m\ell^{-3})(l^2 t^{-2}\theta^{-1}) = m\ell t^{-4}\theta^{-1},\end{aligned} \tag{32}$$

therefore, c_d is dimensionless as both of its numerator and denominator has the same dimension and likewise

$$\begin{aligned}[(\overline{H_c}^2)] &= m\ell^{-1}t^{-2},\\ [\rho c_n(T_c)T_c] &= (m\ell^{-3})(\ell^2 t^{-2}\theta^{-1})(\theta) = m\ell^{-1}t^{-2},\end{aligned} \tag{33}$$

so c_s is also dimensionless for the same reason.

Theory of electron contribution to thermal conductivity of superconductors, which we take into account in this work by ignoring phonon contribution, has been investigated in [48] where based on BCS theory the formulation

$$k(T) = \frac{k_{es}(T)}{k_{en}(T)} = \frac{f(-y) + y\ln(1+e^{-y}) + y^2/2(1+e^y)}{f(0)} \tag{34}$$

was tested in [49] with experimental values of niobium alloys, where

$$f(-y) = \int_0^\infty \frac{z\,dz}{1+e^{z+y}}, \tag{35}$$

and

$$y = \Delta(T)\Delta(0)/k_B T_c T = a\Delta(T)/T, \text{ with } a = \Delta(0)/k_B T_c.$$

Here k_B is the Boltzmann constant and $\Delta(T)$ is the nondimensional energy gap in BCS theory [48](Fig 1., page 1186) with an approximation

$$\Delta(T) \doteq \tanh(c(1/T-1)^{1/2}) \tag{36}$$

known as *semi-empirical interpolation formula*, which is used as a convenient approximation to $\Delta(T)$ for temperature values in $(0,1]$, the reason for using this approximation is that $\Delta(T)$ in BCS theory is defined by a singular integral equation that requires extensive numerical computations. We take $c = 1.87$ which is usually in the range $[1.85, 1.9]$ for niobium.

As it stands, use of (34) for $k(T)$ is also not numerically effective, therefore we propose the following approximation which complies with the experimental values of a niobium alloys [49], Fig. 1(left) with $a = 1.83$ in (35), noting that for niobium $2a = 2\Delta(0)/k_B T_c = 3.65 \pm 0.04$ [50].

$$k(T) = \begin{cases} 3T^3, & T < 1/2\\ 0.38 + (T-0.5)(1.7 - 1.53(T-0.7)), & 1/2 \le T < 1\\ 1, & T \ge 1\end{cases} \tag{37}$$

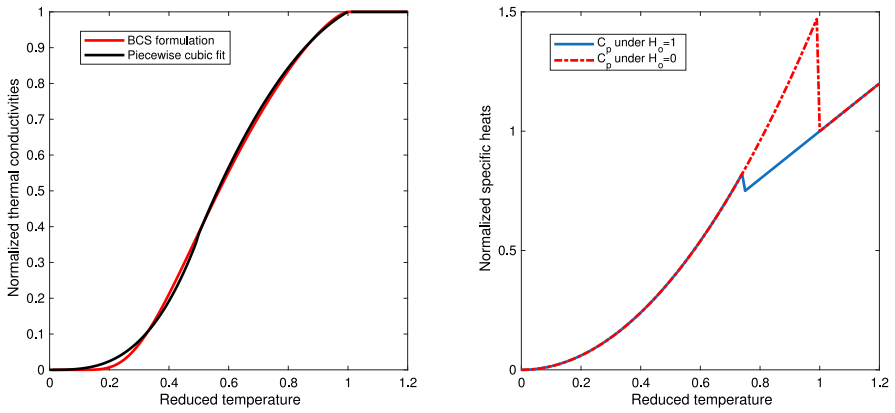

Fig. 1. Thermal conductivity(left) and specific heat(right) versus reduced temperature adapted from [49], [48](left) and [1], [3], [51] (right).

We also use a nondimensional fit to mixed state specific heat under applied field for a niobium alloy [51] Fig. 1(right) as

$$c_p(T) = \begin{cases} 2.5T^2 & T < 3/4 \\ T & T \geq 3/4 \end{cases} \tag{38}$$

As for the boundary conditions, we have

$$\left(\frac{i}{\kappa(T)}\nabla + \mathbf{A}\right)\Psi \cdot \mathbf{n} = 0, \tag{39}$$

$$(\nabla \times \mathbf{A}) \times \mathbf{n} = \mathbf{H}_o \times \mathbf{n}, \tag{40}$$

$$-k(T)(\nabla T \cdot \mathbf{n}) = h_t(T - Tout) \tag{41}$$

on $\Gamma \times (0, \infty)$. Condition (39) implies that no supercurrent is allowed to flow through the boundary of the sample, and condition (40) indicates that the induced magnetic field along the boundary is equal to the applied field $\mathbf{H}_0$, where $\mathbf{n}$ represents the outward unit normal vector to the boundary of $\overline{\Omega}$ denoted by Γ. Finally, (41) is the usual convection boundary condition where we assume $T_{out} = 0$ and h_t is the heat transfer coefficient, which is assumed to be constant.

Furthermore, the HTDGL system (15)–(41) at the initial time, must be supplemented with the initial conditions

$$\Psi(\mathbf{x}, 0) = \Psi_0(\mathbf{x}), \quad \mathbf{A}(\mathbf{x}, 0) = \mathbf{A_0}(\mathbf{x}), T(\mathbf{x},0)=T_0(\mathbf{x}), \mathbf{x} \in \overline{\Omega} \tag{42}$$

Our aim is to analyse both transient, as well as the stationary state, of (15)–(42). Outline of some closely relevant literature(not the complete list, unfortunately) is given in Table 1.

We note that (15)–(42) can be reduced from a model for non-isothermal superconductivity, derived independently by G. Maugin, and K. Miya [35] and S. A. Zhou [36] as described and further analysed in Philips [37] with equations $(1.1) - (1.5)$ in zero potential gauge with $\Phi = 0$, $g(T) = T$ and $b_1 = c_1 = 0$, and constant physical parameters except for Neumann thermal boundary condition, we use convective boundary condition to simulate both zero-field and field-cooling procedures.

4. Spatial discretization of HTDGL

To keep gauge invariant property of the functional (11), bond variables(see for example [15]) defined by

$$w = e^{i\kappa(T)\int^x A(\zeta,y)d\zeta}, v = e^{i\kappa(T)\int^y B(x,\eta)d\eta},$$

are introduced in nonstandard spatial discretization, resulting in a heat-coupled system(HTDGL) that can be written as(with $\sigma_n = 1$)

$$\begin{aligned} \Psi_t &= w\left(\frac{1}{\kappa(T)^2}(w^*\Psi)_x\right)_x + v\left(\frac{1}{\kappa(T)^2}(v^*\Psi)_y\right)_y + (1 - T - |\Psi|^2)\Psi, \\ A_t &= A_{yy} - B_{xy} + \frac{1}{\kappa(T)}\mathfrak{F}(\Psi^*\Psi_x) - A|\Psi|^2, \\ B_t &= B_{xx} - A_{yx} + \frac{1}{\kappa(T)}\mathfrak{F}(\Psi^*\Psi_y) - B|\Psi|^2, \\ (c_p(T)T)_t &= c_d\left[\left(k(T)T_x\right)_x + \left(k(T)T_y\right)_y\right] + c_o\left(A_t^2 + B_t^2\right) \end{aligned} \tag{43}$$

where $\mathfrak{F}(.)$ represents imaginary part of its argument. Following [30], the second-order spatial discretization of (43) can be written as

$$\frac{dU}{dt} = F(U) \tag{44}$$

Table 1
A brief overview of some Heat-coupled Ginzburg–Landau Models.

Ref.	Heat equation source term components	Geometry, Thermal Boundary Cond.	Thermal Coupling	c, κ, k	Outline of work
[33]	$\|\Psi\|, \|\Psi\|_t$	$\Omega \subset R^3$ Dirichlet	ignores electromagnetic effects, thermal coupling through $\|\Psi\|$	const.	maximum principle for $\|\Psi\|$
[34]	$\|\Psi\|, \|\Psi\|_t$	$\Omega \subset R^3$ Dirichlet	ignores electromagnetic effects, thermal coupling through $\|\Psi\|$	const.	existence and uniqueness
[37]	$\|\Psi\|_t$, $\mathbf{A}_t$, $\Psi^*, \Psi_t, \nabla T$	$\Omega \subset R^3$ Neumann	thermal coupling of Maxwell eqn. is indirect	const.	existence, uniqueness and long time behaviour
[38]	$\|\Psi\|^4, \|\Psi\|^2$	convective boundary conditions for 1/T	thermal coupling of Maxwell eqn. is indirect	const.	global existence of classical solutions
[39]	$\mathbf{J}_n \cdot \mathbf{E}$	thin film, heat absorption	thermal coupling of electrostatic potential is indirect	const.	effect of heat dissipation on hysteresis in current–voltage characteristics
[40]	$\mathbf{J}_n \cdot \mathbf{E}$	thin film, heat absorption	thermal coupling of Maxwell eqn. is indirect	const.	collisions between vortices resulting in Joule heat
[41]	$\mathbf{J}_n \cdot \mathbf{E}, \|\Psi_t\|^2, \|\Psi\|_t^2$	thin film, heat absorption	thermal coupling of Maxwell eqn. is indirect	const.	thermal coupling has an effect on vortex motion
[42]	$\mathbf{J}_n \cdot \mathbf{E}, \|\Psi_t\|^2, \|\Psi\|_t^2$	Three dimensional sample, Dirichlet and convective	thermal coupling of Maxwell eqn. is indirect	const.	effect of heat diffusion on resistive state
This work	$\mathbf{J}_n \cdot \mathbf{E}$	cross-section of $\Omega \subset R^3$, convective boundary cond. for T	thermal coupling of Maxwell eqn. is through $\kappa(T)$	experi-mental(Nb) $c(T)$, $k(T)$, $\kappa(T)$	FC and ZFC with hexagonal pattern, thermal hysteresis

where

$$U := (\Re(\Psi), \Im(\Psi), A, B, T). \tag{45}$$

is an array of $N_{xm} \times N_{ym}$ matrices containing unknowns in the interior grid points, $N_{xm} = N_x - 2, N_{ym} = N_y - 2$. The last equation in (44), which did not exist in our previous works, is discretized with respect to space variables as

$$\frac{d(c_p(T)T)}{dt} = c_d \left(\nabla_x(k(T)\Delta_x T) + \nabla_y(k(T)\Delta_y T)\right) + c_o \left((dA/dt)^2 + (dB/dt)^2\right) \tag{46}$$

where $\Delta_x, \Delta_y(\nabla_x, \nabla_y)$ are forward(backward) derivative operators, i.e.,

$$\Delta_x T = \frac{\overline{T} - T}{h_x}, \nabla_x T = \frac{T - \overline{T}}{h_x}, \Delta_y T = \frac{T^{\uparrow} - T}{h_y}, \nabla_y T = \frac{T - T^{\downarrow}}{h_y}$$

Finally, we discretized convective boundary condition given by (41) using second-order difference approximation to the gradient, where $k(T)$ was computed at the centre of cells.

We extend the very effective method called 'the method of planes' that we introduced in [43,44] to Semi-discretized HTDGL defined by (44) in a straightforward way:

- *Define relevant computational and physical parameters*
- *Form an array of matrices from initial conditions*

$$(\Re(\Psi(0)), \Im(\Psi(0)), A(0), B(0), T(0)),$$

each with a dimension of (N_{xm}, N_{ym}), *and call it* $U(0)$.

- *Form U_v as column vector of length $5N_{xm} \times N_{ym}$ corresponding to $U(0)$.*
- *Pass U_v as an initial condition to a high order scheme of ODESUITE [45] for (44) with an appropriate time span of length one.*
- *Extract $U = (\Re(\Psi), \Im(\Psi), A, B, T)_{5N_{xm} \times N_{ym}}$ from U_v and compute boundary values to form extended array $U_g = (\Re(\Psi), \Im(\Psi), A, B, T)_{5N_x \times N_y}$ which contains boundary values as well.*
- *Compute $F(U_g)$ with no use of loops, using only matrix algebra of MATLAB. Note that due to second derivative operators $F(Ug)$ becomes an array of $(5N_{xm}, N_{ym})$ matrices.*
- *From $F(U_g)$, form column vector $F_v(U_g)$ of size $5N_{xm} \times N_{ym}$ and integrate the system (44) over a given time span with ODESUITE.*
- *Repeat the last four steps until a stationary state is achieved, which is measured by GL energy of consecutive states of the system, namely the difference between new energy and energy from previous step being less than a threshold$(here 0.1)$ or number of iterations less than $Max_iter(here 4000)$, allowing it to run in case where energy may increase.*

A comparative performance analysis of solvers in ODESUITE was carried out in [44] for the isothermal version of the model presented here and was found that *ode113* was the most effective, although the transient behaviour of the solution was independent of the particular solver chosen. As it stands, the highly nonlinear system (44) is numerically challenging over a computational domain of size $L_x = L_y = 20$ with $N_x = N_y = 250$, grid points. However, the highly effective algorithm described above, which implements the method of planes with ODESUITE, allows us to reach the equilibrium in a reasonable time on a PC with a CPU of 3.20 GHz, which, earlier, we had to use supercomputers even for the isothermal case [26].

5. Numerical simulations

5.1. Temporal evolution of thermo-electromagnetic state during transition to a mixed state in zero-field cooling(ZFC)

In this numerical experiment, we would like to observe coupled thermal and electromagnetic state(i.e. thermo-electromagnetic state) of sample, initially cooled in the absence of applied field, during transition to mixed state. We initially set reduced temperature $T(x, 0) = 0.1$, that is, we assume that initially the sample is placed at a temperature close to model temperature of absolute zero and exposed to outer temperature $T_{out} = 0$ and is allowed to further cool down via convection boundary condition (41) with $h_t = 2$. We also assume that the sample is initially in superconducting state with no field

$$\Re(\Psi(\mathbf{x}, 0)) = 1, \Im(\Psi(\mathbf{x}, \mathbf{0})) = \mathbf{A}(\mathbf{x}, 0) = \mathbf{0}, \mathbf{x} \in \overline{\Omega}$$

and, we set $\kappa(0) = 5$(niobium sample in dirty limits); and thermal diffusion and ohmic heat coefficients to $c_d = 2, c_s = 1$, respectively. Then we apply magnetic field along the $z-$direction with strength of $H_o = 1$ and observe simultaneous thermo-electromagnetic state as the field enters in the form of flux lines, simulating transition to mixed state, governed by heat-coupled system (43). In Fig. 2, we display superelectron density, represented by $|\Psi|^2$, on the first and third columns and reduced temperature on the second and fourth columns during the transition to a mixed state at the indicated time values. We note that in the subplot for nondimensional time value of $t = 5$, temperature ranges approximately in the interval $[0.15, 0.35]$ resembling a paraboloid that takes smaller values around the centre of the sample. Magnetic field exposure leads to increase of temperature from the initial value of 0.1 up to 0.35 around the edges where normal current begins to flow in a counter clockwise direction. Density of superconducting electrons form almost a constant plane of height 0.7 away from the edges and approaches zero towards the edges where field enters. In the subplot for $t = 50$, we observe development of vortices through the corners with a beautiful symmetry with induced field in between and relatively cooler region around the edges of the sample. In the subplot for $t = 100$, we observe more vortices aligned symmetrically with respect to coordinate system having the origin at the centre of the sample with temperature about 0.25 which is higher than the initial value around the centre. In the subplot for $t = 500$, temperature seems to have fallen to the range of $[0.04, 0.1]$ from the previous range of $[0.1, 0.3]$. In the subplot from $t = 1000$ up to the stationary state at $t = 10000$, we observe that temperature decreases through the edges(second and fourth columns) and vortices are aligned to form mostly hexagonal patterns where final temperature ranges in the interval of $[0.04, 0.1]$.

5.2. Temporal evolution of thermo-electromagnetic state during transition to a mixed state in field-cooling(FC)

In this numerical experiment, we would like to observe thermo-electromagnetic state of sample during transition to mixed state as sample cools down. We initially set reduced temperature $T(x, 0) = 1$, that is, we assume that initially the sample is placed at critical temperature and exposed to outer temperature $T_{out} = 0$ and is allowed to cool down via convection boundary condition (41) with $h_t = 2$. We also assume that the sample is initially almost in normal state with no field

$$\Re(\Psi(\mathbf{x}, 0)) = 1E-3, \Im(\Psi(\mathbf{x}, \mathbf{0})) = \mathbf{A}(\mathbf{x}, 0) = \mathbf{0}, \mathbf{x} \in \overline{\Omega}$$

and, we set $\kappa(0) = 5$; and thermal diffusion and ohmic heat coefficients to $c_d = 2, c_s = 1$, respectively. Then we apply magnetic field along the $z-$direction with strength $H_o = 1$ and observe simultaneous thermo-electromagnetic state as the sample cools down and field enters in the form of flux lines, simulating transition to mixed state, governed by heat-coupled system (43).

In Fig. 3, we display superelectron density on the first and third columns and reduced temperature on the second and fourth columns during the transition to a mixed state at the indicated time values. We note that in the subplot for nondimensional time value of $t = 5$, temperature ranges approximately in the interval $[0.4, 0.8]$ resembling a paraboloid whose larger values are around the

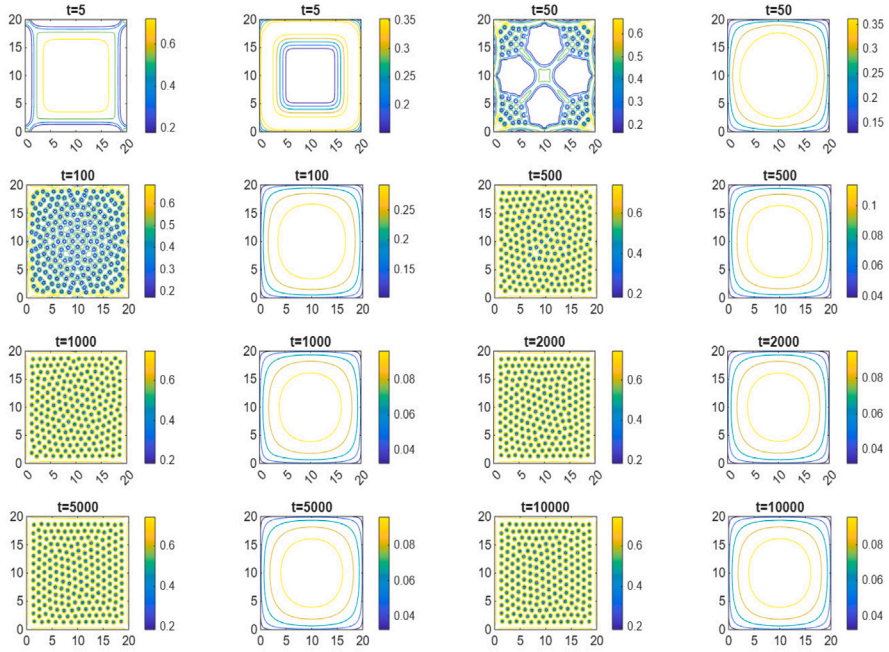

Fig. 2. Zero-field cooling with HTDGL(superelectron density(first and third column), reduced temperature(second and fourth column)).

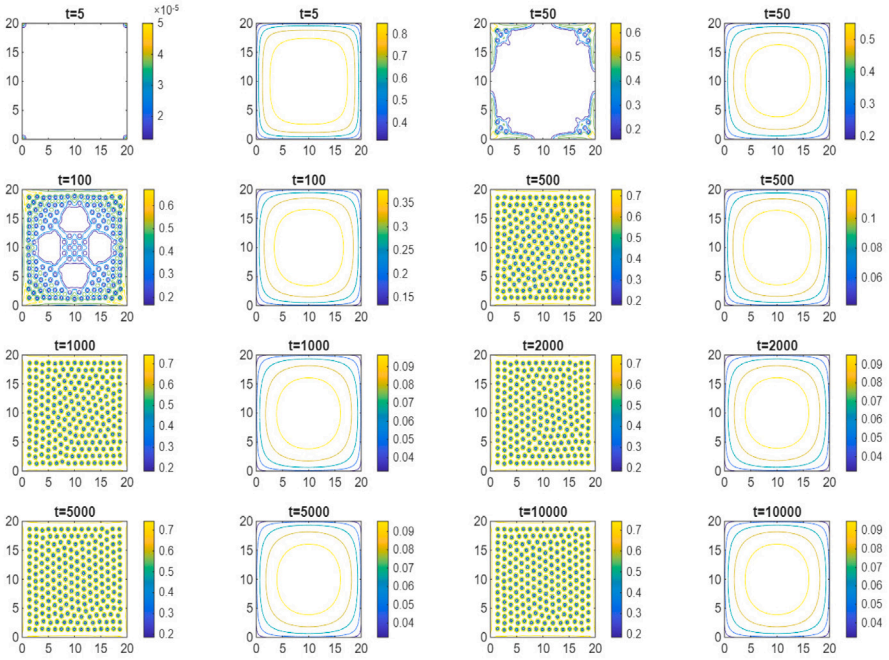

Fig. 3. Field-cooling with HTDGL(superelectron density(first and third column), reduced temperature(second and fourth column)).

centre of the sample while vortices begin to nucleate through the corners. In the subplot for $t = 50$, we observe vortex development through the corners and further temperature reduction down to range of $[0.2, 0.5]$. In the subplot for $t = 100$, we observe more symmetrical vortices being developed around the corners and edges, as well as the centre while temperature reduced further down to the range of $[0.15, 0.35]$. In the subplot for $t = 500$, we observe mixed state with vortices of no certain pattern and further reduction of temperature to the range of $[0.06, 0.1]$. For the remaining time values up to the stationary state at $t = 10000$, temperature equilibrates in the range $[0.04, 0.09]$ where mostly hexagonal patterns dominate.

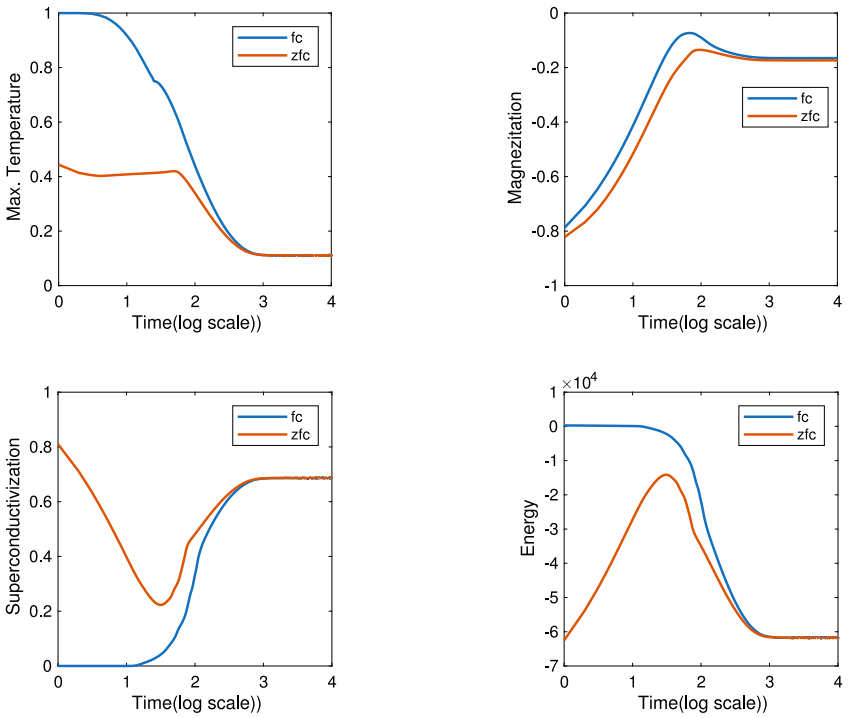

Fig. 4. Field-cooling vs zero-field-cooling with HTDGL.

Note that for both *zero-field-cooled* and *field-cooled* procedures, temperature in the sample at the stationary state varies in the range of $[0.04, 0.09]$ with inner regions having larger values and, unlike the expectations, does not tend to outer temperature value $T_{out} = 0$. This behaviour is attributed to the fact that both thermal conductivity $k(T)$ and specific heat $c(T)$, see Fig. 1 , as well as the source term in (23) tends to zero for large time values at which temperature assumes low values which prevents further heat conduction through the regions near the boundary of the sample.

5.3. A comparative transient behaviour of field-cooled vs zero-field-cooled procedures

In Fig. 4, we display transient behaviour of Maximum temperature; Magnetization, defined as $\langle \mathbf{B} \rangle - H_o$, where $\langle . \rangle$ stands for the spatial average of the quantity inside; superconductivization, which we define as $\langle |\Psi|^2 \rangle$ and GL Energy for both *field-cooled* and *zero-field-cooled* procedures on logarithmic timescale.

In both procedures, maximum temperature tends to 0.1 as the sample reaches at the equilibrium state. Note a small discontinuity in the derivative of maximum temperature curve(blue,in FC) in the logarithmic time interval of $[1, 2]$, which is attributed to discontinuity in $c_p(T)$. In FC procedure the initial maximum temperature of $T = 1$ almost remains so till time $t = 10, log(t) = 1$ then it begins to fall down. In ZFC procedure the initial maximum temperature of $T = 0.1$ rises up to the value of around 0.4 in a relatively short time due to induced normal current flow circulating around the centre, afterwards, it begins to fall down to the same value of that of FC procedure as shown in the upper left subplot.

In magnetization curves we see that although initial magnetic state is the same for both cases, average induced magnetic field becomes larger in the FC state as initial superconducting state around the initial temperature of $T = 0.1$ resists field entry in ZFC to a certain extend. However, the gap tends to close as the system gets closer to stationary state.

The superconductivization curve for FC state is natural as sample change phase from normal to mixed state. In ZFC state, however, vortex interaction around the log time of 1.65 leads to expulsion of some field which results in an increase in superconductivization curve. As system tends to equilibrium, both curves approach the same value.

GL energy curve for FC procedure remains steady for a while till vortices begin to nucleate and then monotonically decreases as in the isothermal case. However, GL energy for ZFC procedure in the Heat-Coupled model is no longer monotonically decreasing which means that, instead of asking for a decreasing GL energy, one should be content only with stationary GL energy representing equilibrium state. Stated in a different way, the GL energy, as it stands, is not in the right form for HTDGL where stationary state seeks to minimize.

Furthermore, to physically compare two configurations we use the measure known as Abrikosov constant defined by

$$\beta_A = \frac{\langle |\Psi|^4 \rangle}{\langle |\Psi|^2 \rangle^2}$$

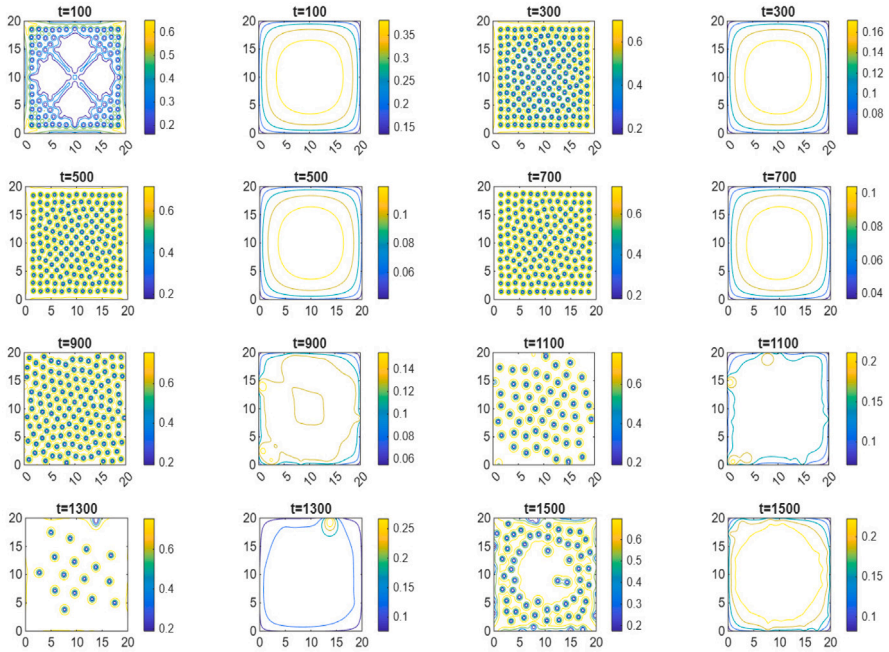

Fig. 5. Evolution of observables in a sample without pinning cites under oscillatory field.

which is conventionally used as a measure for vortex geometry [1](p. 414),[52]. For the above simulations we found that $\beta_A(FC) = 1.08393$ and $\beta_A(ZFC) = 1.08325$. For a perfect hexagonal lattice, it is known that $\beta_A \doteq 1.16$, and for a square lattice $\beta_A \doteq 1.18$ [1] and a lower value of β_A represents a more thermodynamically stable vortex state configuration. Finally we note the resemblance of vortex configurations in both FC and ZFC procedures with that of $NbSe_2$ ([52], Fig. 6, by scanning tunnelling microscopy).

5.4. Hysteresis in a superconductor with pinning sites

In this experiment, at first we introduce pinning sites by penalizing energy functional at pinning sites: namely we redefine local condensation energy as

$$g_{lc} = \begin{cases} (T-1)|\Psi|^2 + \frac{1}{2}|\Psi|^4 & \mathbf{x} \in \boldsymbol{\Omega} \backslash \boldsymbol{\Omega}_{ij} \\ (P+T-1)|\Psi|^2 + \frac{1}{2}|\Psi|^4 & \mathbf{x} \in \boldsymbol{\Omega}_{ij} \end{cases}$$

where we let $P = 200$ and

$$\boldsymbol{\Omega}_{ij} = [x_{i-1}, x_{i+1}] \times [y_{j-1}, y_{j+1}] \tag{47}$$

for $i = 10, 20, \ldots, 240; j = i$ in computational domain $[0, 250] \times [0, 250]$.

Then we define oscillatory applied field by

$$h(t) = \begin{cases} H_0, & 0 \le t < 500 \\ H_0 cos(\pi t/1250 - 2\pi/5) & 500 \le t \le 3000 \end{cases} \tag{48}$$

Here the field allows for sample to enter mixed state by the time $t = 500$ under a constant field H_0, and then field is reduced to $-H_0$ followed by an increase up to the original value of $H_0 = 1$ with $\kappa(0) = 4, c_d = 2, c_s = 1, h_t = 2$ with FC procedure.

Temporal evolution of density of superconducting electrons is displayed in the first and third columns; and that of the temperature is displayed in the second and fourth columns in Fig. 5 in a sample with no pinning sites.

At $(t, h) = (100, 1)$, we observe vortex nucleation through the corners with temperatures in the range of interval $[0.15, 0.35]$, being reduced from the initial value of $T(\mathbf{x}, 0) = 1$, where central portions have larger values. At $(t, h) = (300, 1)$, vortex development stage is completed with temperature falling down to the range of $[0.08, 0.16]$, and at $(t, h) = (500, 1)$ being reduced to $[0.06, 0.1]$ and further down to $[0.04, 0.1]$ at $(t, h) = (700, 0.8763)$. At $(t, h) = (900, 0.5358)$ we see that vortices leaving the sample due to the weaker field strength leads to increase in temperature up to the interval $[0.06, 0.14]$. The pattern repeats itself with the observation that vortices leaving out the system leads to local increase of temperature around such moving vortices up to the range $[0.1, 0.2]$ at $(t, h) = (1500, -0.8090)$.

On the other hand, the results with pinning sites defined by (47) are displayed in Fig. 6. At $(t, h) = (100, 1)$, we observe vortex nucleation through the corners with temperatures in the range of interval $[0.15, 0.35]$, being reduced from the initial value of

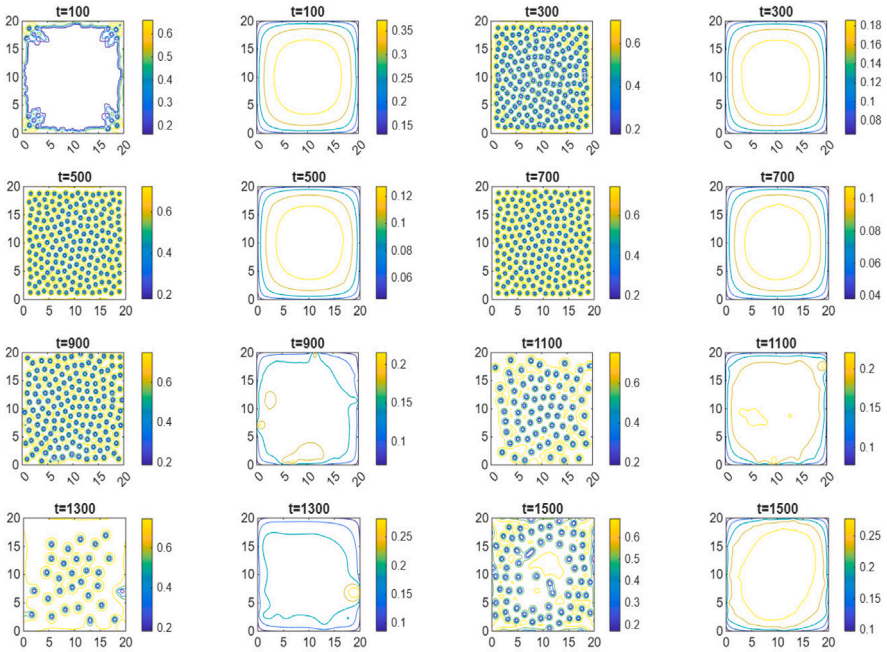

Fig. 6. Evolution of observables in a sample with pinning cites under oscillatory field (48).

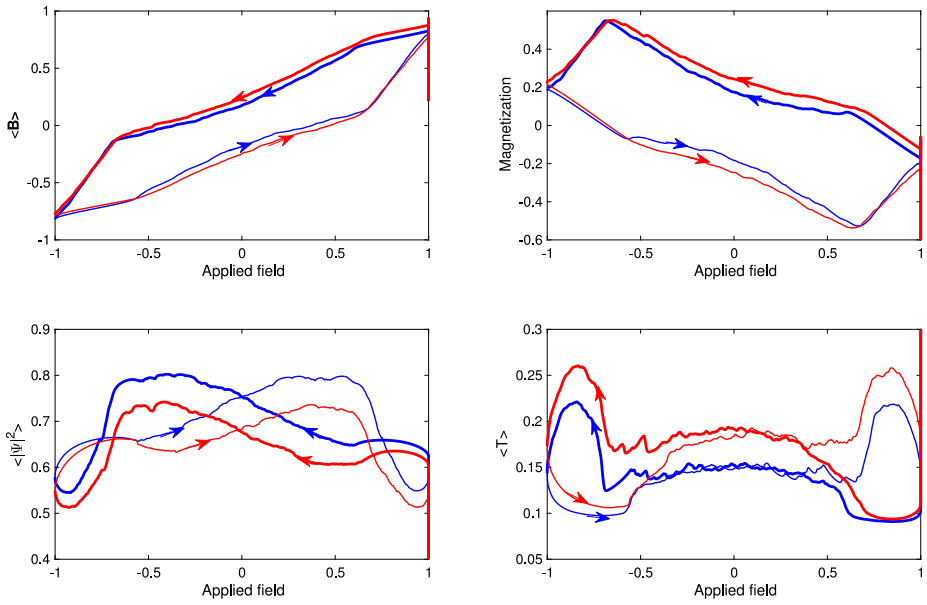

Fig. 7. Evolution of observables in a sample with(red) and without (blue) pinning cites under oscillatory field.

$T(\mathbf{x}, 0) = 1$, where central portions have larger values. Compared to Fig. 5 (top left subplot for $(t, h) = (100, 1)$) we observe that pinning sites have led to a delay in vortex development. We see that sample continues to cool down until $t = 900$. At $(t, h) = (900, 0.5358)$, we see that vortices leaving the sample due to the weaker field strength leads to local increase in temperature around such vortices as in the case of Fig. 5, but the temperature range is relatively higher up to $[0.1, 0.2]$ which is attributed to flux interaction with pinning sites. Due to pinning sites, at $t = 1100$, sample keeps more vortices as compared to Fig. 5 for the same t value with temperature range in $[0.1, 0.2]$. Likewise at $t = 1300$ and $t = 1500$ sample keeps more vortices with relatively higher final temperature range of $[0.1, 0.25]$.

In Fig. 7, we display hysteresis curves in a sample with(red) and without(blue) pinning sites as defined above.

The curves begin from upper right corners with thick lines with applied field $(0, 0, 1)$ and proceed towards the left as the field changes direction to $(0, 0, -1)$ at $t = 1750$ by the function (48). Applied field versus average induced field, $\langle \mathbf{B} \rangle$; Magnetization $\langle \mathbf{B} \rangle - H_o$(up to a scalar factor);average density of superconducting electrons $\langle |\Psi|^2 \rangle$ and average temperature $\langle T \rangle$ curves are displayed for both sample with(red) and without(blue) pinning sites.

Hysteresis is attributed to boundary effects and pinning sites. Larger area of loops for average induced magnetic field and magnetization are observed for the sample with pinning sites as expected, as those sites tend to impede vortex motion and trap flux. As for the curves for $\langle |\Psi|^2 \rangle$, the red coloured curve begins at a value representing almost normal state at the lower right corner and proceeds towards the left remaining under the blue curve due to large number of pinning sites impeding vortex development and motion. The fluctuations or zigzags in the left bottom curve is believed to be due to relative change in the number of vortices corresponding to neighbouring applied field values. The curves representing average temperature versus applied field implies that sample with pinning sites(red curve) remain at larger temperature values in average which is attributed to Joule heating due to interaction with pinning sites. The zigzags in the figure(lower-right) is attributed to thermal fluctuations as applied field changes continuously.

6. Conclusion

In this study we extended the isothermal TDGL model to HTDGL, with Joule heat being the only heat source for the heat equation where temperature dependence of GL parameter, thermal conductivity and specific heat were taken into consideration in terms of general empirical findings of Niobium(dirty limit) superconductors. We integrated numerically the governing equations using the "method of planes" approach introduced in our earlier works. We carried out numerically experiments to examine temporal evolution with ZFC and FC procedures. We observed that in both procedures, the stationary state leads to a hexagonal pattern of vortices with almost the same Abrikosov constant. In ZFC procedure, initial normal current flow due to applied field leads to local increase of temperature near the edges of the sample. Hysteresis curves for a sample with and without pinning sites were also investigated and observed that pinning sites, in addition to known magnetic effects, lead to relatively more local increase of temperature especially during vortex motion leaving the sample under oscillatory field.

Declaration of competing interest

The authors declare that they have no known competing financial interests or personal relationships that could have appeared to influence the work reported in this paper.

Acknowledgements

The author would like to express his sincere gratitude to Professor Man Kam Kwong for introducing him to the fascinating field of superconductivity. The author also gratefully acknowledges the short visit to OCIAM(Oxford Centre for Industrial and Applied Mathematics), supported by TÜBİTAK (The Scientific and Technological Research Council of Türkiye) and the Royal Society through the European Research Scientific Exchange Programme in 2003 upon invitation of Professor John Ockendon, FRS, which played an important role in drawing the author's attention to the research topic of this manuscript. The author also very much appreciates the comments and suggestions of each four of anonymous reviewers and the extra time given for the revision that helped for a better presentation of the work.

Data availability

No data was used for the research described in the article.

References

[1] A.A. Abrikosov, Fundamentals of the Theory of Metals, Elsevier Science, 1998.
[2] C.G. Kuper, An Introduction to the Theory of Superconductivity, Clarendon Press, 1968.
[3] M. Tinkham, Introduction to superconductivity, R. E. Krieger Pub. Co., Florida, 1975.
[4] E. Sandier, S. Sefathy, Vortices in the Magnetic Ginzburg–Landau model, Birkhauser, Boston, 2007.
[5] T. Kita, Statistical Mechanics of Superconductivity, Springer, Japan, 2015.
[6] N.B. Kopnin, Vortex dynamics and mutual friction in superconductors and fermi superfluids, Rep. Progr. Phys. 65 (2002) 1633.
[7] Q. Du, Finite element methods for the time-dependent Ginzburg–Landau model of superconductivity, Comp. Math. Appl. 27 (1994) 119–133.
[8] M. Mu, A linearized Crank–Nicolson-Galerkin method for the Ginzburg–Landau model, SIAM J. Sci. Comput. 18 (4) (1997) 1028–1039.
[9] Z. Chen, S. Dai, Adaptive Galerkin methods with error control for a dynamical Ginzburg–Landau model in superconductivity, SIAM J. Numer. Anal. 38 (6) (2001) 1961–1985.
[10] B. Li, Z. Zhang, A new approach for numerical simulation of the time-dependent Ginzburg–Landau equations, J. Comput. Phys. 303 (15) (2015) 238–250.
[11] W. Chenda, S. Weiwei, Analysis of Galerkin FEMs for mixed formulation of time-dependent Ginzburg–Landau equations under temporal gauge, SIAM J. Numer. Anal. 56 (3) (2018) 1291–1312.
[12] H.D. Gau, L. Ju, W. Xie, A stabilized semi-implicit Euler gauge-invariant method for the time-dependent Ginzburg–Landau equations, J. Sci. Comput. 80 (2019) 1083–1115.
[13] Q. Zhang, H. Duan, Residual-based a posteriori error estimates for the time-dependent Ginzburg-Landau equations of superconductivity, J. Sci. Comp. 93 (2022) 79, http://dx.doi.org/10.1007/s10915-022-02041-0.

[14] E. Coskun, Numerical Analysis of Ginzburg–Landau Models for Superconductivity (Ph. D. Dissertation), Northern Illinois University, De Kalb, IL., USA, 1994.
[15] M.K. Kwong, H.G. Kaper, Vortex configurations in type-II superconducting films, J. Comput. Phys. 119 (1995) 120–131.
[16] E. Coskun, M.K. Kwong, Simulating vortex motion in superconducting films with the time-dependent Ginzburg–Landau equations, Nonlinearity 10 (1997) 579–593.
[17] E. Coskun, Computational simulation of flux trapping and vortex pinning in type-II superconductors, Appl. Math. Comp. 106 (1999) 31–49.
[18] W.B. Richardson, A.L. Pardhanani, G.F. Carey, A. Ardelea, Numerical effects in the simulation of Ginzburg–Landau models of superconductivity, Internat. J. Numer. Methods Engrg. 59 (2004) 1251–1272.
[19] H.M. Jafri, X. Ma, C. Zhao, D. Liang, H. Huang, Z. Liu, L.Q. Chen, Numerical simulation of vortex dynamics in type-II superconductors in oscillating magnetic field using time-dependent Ginzburg–Landau equations, J. Phys.-Condens. Matter 29 (2017) 50.
[20] E. Abrahams, T. Tsuneto, Time variation of the Ginzburg–Landau order parameter, Phys. Rev. 152 (1966) 416.
[21] R.A. El-Nablusi, W. Anukool, On nonlocal Ginzburg-Landau superconductivity and Abrikosov vortex, Physica B 2022, 414229.
[22] C.W.W. Haddon, et al., Computational simulations using time-dependent Ginzburg–Landau theory for Nb-Ti-like microstructures, IEEE Trans. Appl. Supercond. 32 (4) (2022).
[23] K.V. Grigorishin, Extended time-dependent Ginzburg–Landau theory, J. Low Temp. Phys. 203 (2021) 262–308.
[24] E.C.S. Duarte, E. Sardella, W.A. Ortiz, R. Zadorosny, Dynamics and heat diffusion of Abrikosov's vortex-antivortex pairs during an annihilation process, J. Phys. : Condens. Matter 29 (2017) 405605.
[25] M. Doria, J. Gubernatis, D. Rainer, Solving the Ginzburg–Landau equations by simulated annealing, Phys. Rev. B 41 (1990) 6335–6340.
[26] E. Coskun, M.K. Kwong, Parallel Solution of the Time-Dependent Ginzburg–Landau Equations, Technical Report, MCS, $ANL-95/49$, Argonne National Laboratory, Argonne, IL, 1995, https://ftp.mcs.anl.gov/pub/tech_reports/reports/ANL9549.pdf.
[27] N. Galbreath, W. Grop, D. Gunter, G. Leaf, D. Levine, Parallel solution of the three-dimensional time-dependent Ginzburg–Landau equation, in: Proc. SIAM Conf. on Parallel Proc. for Sci. Comp. SIAM, Philadelphia, 1993.
[28] W.D. Gropp, H.G. Kaper, G.K. Leaf, D.M. Levine, M. Palumbo, V.M. Vinokur, Numerical simulation of vortex dynamics in type-II superconductors, J. Comput. Phys. 123 (1996) 254–266.
[29] D. Gunter, H. Kaper, G. Leaf, Implicit integration of the time-dependent Ginzburg–Landau equations of superconductivity, SIAM J. Sci. Comput. 23 (2002) 1943–1958.
[30] E. Coskun, Z. Çakir, P. Takac, Nucleation of vortices with a temperature and time-dependent Ginzburg–Landau model of superconductivity, European J. Appl. Math. 14 (2003) 111–127.
[31] A.V. Harbick, M.K. Transtrum, Time-dependent Ginzburg–Landau framework for sample-specific simulation of superconductors for radio frequency applications, Phys. Rev. B 112 (2025) 094518.
[32] B. Oripov, S.M. Anlage, Time-dependent Ginzburg–Landau treatment of rf magnetic vortices in superconductors: Vortex semiloops in a spatially nonuniform magnetic field, Phys. Rev. E 101 (2020) 033306.
[33] M. Fabrizio, Ginzburg–Landau equations and first and second-order phase transitions, Internat. J. Engrg. Sci. 44 (2006).
[34] M. Fabrizio, B. Valeri, A non-isothermal Ginzburg–Landau model in superconductivity: Existence, uniqueness and asymptotic behaviour, Nonlinear Anal. 66 (2007) 2565–2578.
[35] G. Maugin, Irreversible thermodynamics of deformable superconductors, C. R. Acad. Sci. Paris, T. 314, Sere II (1992) 889–894.
[36] Z.M. Zhou, K. Miya, A nonequilibrium theory of thermoelastic superconductors, Int. J. Appl. Electromag. Mater. 2 (1991) 21–38.
[37] D. Phillips, E. Shin, On the analysis of a non-isothermal model for superconductivity, European J. Appl. Math. 15 (2004) 147–179.
[38] Z. Chen, K.H. Hoffmann, Global classical solutions to a non-isothermal dynamical Ginzburg–Landau model in superconductivity, Numer. Funct. Anal. Optim. 18 (9–10) (2007) 901–920.
[39] D.Y. Vodolazov, F.M. Peeters, M. Morelle, V.V. Moshchalkov, Masking effect of heat dissipation on the current–voltage characteristics of a mesoscopic superconducting sample with leads, Phys. Rev. B 71 (2005) 184502.
[40] K. Kobayeshi, Y. Ota, M. Machida, Numerical experiments of joule heat damage in superconducting transport, Phys. Procedia (2012).
[41] Z. Jing, H. Yong, Y. Zhou, Thermal coupling effect on the vortex dynamics of superconducting films:Time-dependent Ginzburg–Landau simulations, Supercond. Sci. Technol. 31 (2018) 055007.
[42] L.R. Cadorim, L.V. Toledo, E. Sardella, Describing heat dissipation in the resistive state of three-dimensional superconductors, Phys. C: Supercond. Appl. 622 (2024) 1354531, 2024.
[43] E. Coskun, On the properties of a single vortex solution of Ginzburg–Landau model of superconductivity, Phys. A 568 (2021) 125731.
[44] E. Coskun, On the numerical stability and transitional stages of time-dependent Ginzburg–Landau model of superconductivity, Phys. A 626 (2023) 129036.
[45] L.F. Shampine, M.W. Reichert, MATLAB ODE suite, SIAM J. Sci. Comput. 18 (1) (2006) 1–22.
[46] Q. Du, Discrete gauge-invariant approximations of a time dependent Ginzburg–Landau model of superconductivity, Math. Comp. 67 (1998) 965–986.
[47] A. Schmidt, A time-dependent Ginzburg–Landau equation and its application to the problem of resistivity in the mixed state, Phys. Kondens. Mater. 5 (1966) 302–317.
[48] J. Bardeen, L.N. Cooper, Schrieffer, Theory of superconductivity, Phys. Rev. 108 (5) (1957).
[49] F. Koechlin, B. Bonin, Parametrization of the niobium thermal conductivity in the superconducting state, Supercond. Sci. Technol. 9 (1996) 453–460.
[50] V. Novontny, P.P.M. Meincke, Single superconducting energy gap in pure niobium, J. Low Temp. Phys. 18 (1/2) (1975).
[51] A. Mirmelstein, et al., Mixed-state specific heat of the type-II superconductor $Nb_{0.77}Zr_{0.23}$ in magnetic fields up to B_{c2}, J. Supercond. 10 (5) (1997).
[52] A.A. Abrikosov, Nobel lecture: Type-II superconductors and the vortex lattice, Rev. Modern Phys. 76 (3) (2004).